Efficient Orbit Information Dissemination for Energy-Constrained Direct-to-Satellite IoT Systems

Santiago M. Henn[*‡] Juan A. Fraire[*†‡] Gregory F. Stock[‡] Holger Hermanns[‡]

[*]Universidad Nacional de Córdoba, Córdoba, Argentina

[†]Inria, INSA Lyon, CITI, UR3720, 69621 Villeurbanne, France

[‡]Saarland University, Saarland Informatics Campus, Saarbrücken, Germany

Energy-constrained Direct-to-Satellite IoT (DtS-IoT) devices operating over sparse Low Earth Orbit (LEO) constellations require sufficiently accurate satellite orbit knowledge to predict access intervals and efficiently manage channel usage. Disseminating such information over heavily constrained communication links, however, remains a fundamental challenge. This difficulty has been exacerbated in recent years by the rapid growth in the number of active satellites, which has increased the frequency of orbit maintenance and collision-avoidance maneuvers, further degrading orbit predictability beyond the uncertainties introduced by nonlinear perturbed dynamics. This work proposes a lookup-table-based orbit information update scheme that minimizes the transmitted data volume while preserving access-interval prediction accuracy under constrained channel conditions. The proposed approach explicitly accounts for the degradation in orbit-state predictability caused by maneuvering, characterizing access-interval prediction errors as functions of update rate and information granularity. Numerical evaluations and simulation results show that the proposed scheme achieves access-prediction errors comparable to those of full-element dissemination while reducing payload size, demonstrating its effectiveness for low-power DtS-IoT systems.

1 Introduction

Direct-to-Satellite (DtS) communications enable connectivity in remote and underserved regions where terrestrial infrastructure is unavailable or impractical. In the context of the Internet of Things (IoT), Low Earth Orbit (LEO) constellations provide long-range, low-power links for applications such as agriculture, environmental monitoring, and asset tracking [15, 28]. Recent growth in LEO deployments, however, has increased orbital congestion and maneuver frequency, reducing long-term orbit predictability [4, 22].

DtS-IoT devices are typically energy-constrained and experience sparse connectivity, with satellite visibility limited to short passes (on the order of minutes). To conserve energy, ground terminals must activate their radios only during predicted access intervals. This requirement makes accurate orbit knowledge at the device level essential: early activation wastes energy, while late activation results in missed transmission opportunities [15].

Most visibility prediction methods assume frequent orbit updates enabled by persistent connectivity or high-capacity links [13, 17]. Such assumptions are incompatible with low-power DtS-IoT terminals operating under severe downlink constraints. Classical orbit-determination approaches are likewise impractical due to their hardware and data requirements [8]. Meanwhile, increasing maneuver activity further accelerates the obsolescence of orbit information.

Despite extensive work on access prediction algorithms, limited attention has been paid to the efficient dissemination of orbital information to constrained devices. Existing strategies typically rely on transmitting full orbital states or frequent updates, which are ill-suited to narrowband, energy-limited links.

Submitted to:
ETAPS 2026 – MISSION Workshop

This work addresses this gap by proposing a broadcast-assisted orbit update scheme tailored to DtS-IoT systems. The approach leverages compact representations and orbit-family enumeration to minimize the amount of data transmitted while preserving access-interval prediction accuracy under maneuver-driven uncertainty.

The main contributions are:

- A compact, lookup-table-based orbit dissemination scheme for constrained DtS-IoT devices.
- An analysis of access prediction error as a function of update rate and information granularity under maneuver activity.
- Numerical validation showing that orbit-family enumeration maintains prediction accuracy at significantly reduced payload sizes.

2 Background

Low-power, low-data-rate satellite data collection systems have existed for decades. Early examples include ARGOS [5] and traditional Data Collection Systems (DCS) [9], which enabled environmental monitoring in remote areas. However, these systems were not designed to interoperate with modern terrestrial LPWAN technologies such as LoRaWAN and NB-IoT [25].

A major step toward direct-to-satellite IoT (DtS-IoT) was the launch of LacunaSat in 2019, the first LoRaWAN-enabled satellite system, which validated the DtS-IoT communication model [32]. Subsequent deployments, including satellites based on Spire's LEMUR platform, target low-power sensing applications in remote energy and agricultural use cases [20, 33]. Experimental and analytical studies have further demonstrated the feasibility of LoRa-based LEO links, addressing long-range performance, Doppler effects, and waveform adaptations [10–12, 26].

Accurate prediction of satellite visibility intervals has long been central to mission analysis. Classical analytical methods derive rise and set times from orbital geometry [2, 13, 27], while more recent approaches rely on numerical, interpolation-based, or hybrid techniques to balance fidelity and computational cost [1, 16–19, 31]. Recent work has also explored lightweight visibility prediction with autonomous updates for constrained ground nodes [24].

2.1 Limitations of Existing Approaches

Most visibility prediction frameworks assume frequent orbit updates enabled by persistent connectivity or dense constellations. Conventional orbit determination methods further require specialized hardware and extensive observations, making them unsuitable for low-cost, energy-constrained devices [6, 8]. Additionally, increasing maneuver frequency and collision-avoidance operations degrade orbit predictability beyond the effects of natural perturbations.

Commercial constellations, such as Starlink, rely on high-power terminals and continuous coverage [30]. In contrast, DtS-IoT systems (e.g., Lacuna's LS200) are designed for ultra-low-power, multi-year battery operation [14, 21], where frequent, high-volume orbit updates are impractical.

The core challenge, therefore, is not orbit determination but efficient dissemination and use of orbit information under severe communication and energy constraints. The objective is to minimize the amount of transmitted data while preserving access-prediction accuracy, explicitly accounting for maneuver-induced uncertainties that accelerate information obsolescence.

3 Problem Statement

3.1 Scenario Description

We consider a scenario in which End Devices are deployed in remote and isolated locations and must communicate directly with a gateway hosted on board a LEO satellite. As the gateway is part of the satellite payload, its position relative to a given device, and therefore the DtS access intervals, are governed by orbital dynamics.

LEO satellites travel at velocities of up to approximately 7.5 km/s, causing the satellite footprint over the Earth's surface to drift rapidly [3]. As a result, access windows for a given End Device are typically limited to a few minutes per pass. Prediction errors on the same order as the access duration may lead to severely reduced communication opportunities or even completely missed passes [36]. Conversely, compensating for uncertainty by enlarging the predicted access window forces the device to remain active longer than necessary, increasing energy consumption, an unacceptable trade-off for energy-constrained IoT terminals.

3.2 Orbit Information Requirements

To enable an End Device to predict satellite access intervals autonomously, it must be provided with sufficient information to propagate the satellite orbit and compute its position over time. This information constitutes the *orbit information payload*.

A satellite trajectory is fully described by six independent parameters. While Cartesian position and velocity vectors may be used for orbit propagation, orbital elements are widely adopted due to their compact representation and their suitability for modeling orbital perturbations. The six classical orbital elements characterize the orbit size, shape, and orientation; however, the satellite position is inherently time-dependent. Consequently, a time reference (epoch) must be associated with the orbital elements. Additionally, in multi-satellite scenarios, a satellite identifier is required to uniquely associate the orbital data with a specific satellite.

Altogether, orbital elements, their associated epoch, and a satellite identifier constitute the minimum set of information required to propagate the orbit and predict access intervals, resulting in eight fundamental information components.

3.3 Orbit Propagation and Dissemination

Higher propagation accuracy typically entails higher computational cost. The *Simplified General Perturbations 4* (SGP4) model [34, 35] provides a practical compromise and is widely used in operational systems, including IoT-enabled satellite links [7]. SGP4 propagates satellite states in an Earth-centered inertial frame, modeling dominant perturbations such as Earth's oblateness and simplified drag. Typical position errors are on the order of ∼1 km at epoch, growing by ∼1–3 km/day without updates. The model relies on Two-Line Element (TLE) sets as input. Although TLEs include auxiliary parameters beyond the minimum required for position approximation, a compliant TLE can be reconstructed locally if the essential orbital elements are transmitted, avoiding the overhead of sending the full ASCII representation. For reference, a standard TLE is depicted in Table 1. Even without additional metadata, this representation exceeds 130 bytes in ASCII, not accounting for framing overhead.

Table 1: Example TLE set for the LacunaSat mission.

```
LACUNA-4
1 99999U          26021.62500000  .00016900  00000-0  12682-2 0 00009
2 99999 097.6561 097.9879 0012071 090.4217 242.0308 15.02588062000011
```

3.4 Payload Size Constraints

The objective is to minimize the number of bits required to disseminate orbital information, or at least reduce its overhead within a larger transmission frame. In LPWAN systems, payload capacity is tightly constrained. For LoRa, the maximum payload depends on the spreading factor (SF): SF7–SF8 support up to ~222 bytes, SF9 up to ~115 bytes, and SF10–SF12 typically ~51 bytes. In NB-IoT, typical limits are ~160 bytes for uplink (NPUSCH) and ~680 bytes for downlink (NPDSCH). Under such constraints, transmitting a full TLE in ASCII format is inefficient, especially at high spreading factors.

Time and Identifier Encoding. Orbital elements must be associated with a reference epoch. A 32-bit Unix timestamp (seconds since 1970) provides a simple baseline, though mission-specific epochs (e.g., launch date) can reduce bit requirements. Each satellite is encoded using $b = \lceil \log_2(N_s) \rceil$ bits for a constellation of N_s spacecraft.

Orbital Elements Encoding. Element precision directly impacts prediction accuracy. As a practical baseline, allocating 16 bits per Keplerian element results in 96 bits for the six elements. This represents a conservative trade-off between payload size and propagation fidelity and serves as the reference full-state encoding in this work.

Baseline Orbital Dissemination Frame. Aggregating the contributions of the timestamp (32 bits), the orbital elements (96 bits), and the satellite identifier yields a baseline frame size of $128 + \lceil \log_2(N_s) \rceil$ bits. For example, a constellation consisting of $N_s = 16$ satellites requires a total of 132 bits, corresponding to approximately 30% of the maximum payload available at spreading factors SF10–SF12.

4 Dissemination Strategy

The proposed dissemination strategy follows a two-fold approach. First, it relies on a set of well-defined assumptions that allow certain orbital parameters and configuration details to be simplified or inferred directly at the End Device, thereby reducing the amount of information that must be explicitly transmitted. Second, it introduces an enumeration-based mechanism in which a family of candidate orbits is precomputed at both the satellite gateway and the End Device, starting from a commonly agreed-upon reference orbit.

4.1 Strategy Assumptions

These assumptions reflect common operational practices in low-power remote sensing and satellite missions, while some may be interpreted as heuristic, reasonable operational alternatives are discussed where relevant.

End Device Assumptions. From the End Device perspective, we assume: (i) a known and fixed geographic location; (ii) a locally synchronized clock with negligible short- to medium-term drift; (iii) prior knowledge of the mission reference orbit; and (iv) awareness of the agreed orbit enumeration strategy. Reference orbit updates, if required, are disseminated through dedicated control frames or predefined rules.

Satellite Assumptions. From the satellite perspective, we assume: (i) sufficiently accurate onboard orbit knowledge (e.g., via ground updates or GNSS); (ii) a near-circular LEO orbit; and (iii) consistency with the End Devices regarding the reference orbit and enumeration strategy.

Mission Assumptions. The mission operates around a predefined target orbit selected to meet coverage and performance objectives (e.g., Sun-synchronous or repeating ground-track regimes [36]). In near-circular LEO, altitude and inclination govern secular RAAN drift, while atmospheric drag drives altitude decay. Overall, the nominal orbital evolution is known *a priori*, and the spacecraft is maintained within a bounded region of this regime through predictable perturbations and periodic maneuvers.

4.2 Mechanisms

The proposed dissemination mechanism relies on two key ideas: (i) a reduced orbital parametrization enabled by mission-specific assumptions, and (ii) an enumeration-based indexing strategy over a precomputed family of admissible (approximate) orbits.

Orbital Simplification. Under the assumption of near-circular operation, the orbit eccentricity can be neglected. In this regime, the argument of perigee becomes undefined and can be omitted without loss of positional information. The satellite position along the orbital plane is instead parameterized using the *argument of latitude*, defined as the sum of the argument of perigee and the true anomaly. This approximation removes two classical orbital elements from the dissemination payload, reducing both data volume and computational complexity at the End Device.

Orbit Family Construction and Enumeration. Given a commonly agreed reference orbit, a discrete family of admissible orbits is generated by perturbing selected orbital elements within mission-dependent bounds. Each orbit in this family is deterministically indexed using a shared enumeration strategy implemented identically at both the satellite and the end device.

Upon reception of an index, the End Device may recover the corresponding orbit either by: (i) iterating through the generated family until the matching index is found, resulting in a worst-case complexity of $O(N)$ for N orbits, or (ii) performing a constant-time lookup using a pre-populated lookup table with $O(1)$ amortized access time. The choice between these approaches depends on whether the device is more constrained by memory or by computational resources.

At the satellite side, the dissemination process consists of selecting the orbit in the family that best matches the current estimated orbital state. This selection can be implemented by quantizing or rounding the relevant orbital elements to the nearest permissible values within the predefined sets.

Orbit Family Size. The size of the orbit family is strongly mission-dependent, as different operating orbits experience different secular and periodic perturbations. For instance, the secular drift of the RAAN due to the Earth's J_2 perturbation is monotonic and direction-dependent. In prograde orbits, the RAAN

Algorithm 1 Orbit dissemination procedure from the satellite

Require: Current state O_{true}
Require: Current time T, Satellite ID S_{id}
Satellite broadcast
$O_{approx} \leftarrow \text{SIMPLIFYORBIT}(O_{true})$
$e \leftarrow \text{ENUMERATEORBIT}(O_{approx})$
$F \leftarrow \text{ASSEMBLEFRAME}(e, S_{id}, T)$
$\text{BROADCAST}(F)$

Algorithm 2 Frame reception and orbit determination procedure from the device

Require: Device d with local orbit database $\mathcal{D}$
Require: Last known satellite orbital state O_{true}
Require: Current time T, Device position P
Ensure: Device-predicted access intervals I_{device}
Ensure: Next access interval $i_{\text{next}} \in I_{\text{device}}$
Device update by enumeration
if T in i_{next} **then** $\text{RECEIVE}(F)$
  if $e \neq \text{ENUMERATEORBIT}(d.O_{last})$ **then**
    $O_{new} \leftarrow \mathcal{D}.\text{LOOKUP}(e)$
    if $O_{new} \neq \varnothing$ **then**
      $d.O_{last} \leftarrow O_{new}$
Recompute future access prediction
$I_{\text{device}} \leftarrow \text{PREDICTACCESS}(P, d.O_{last})$
$\text{UPDATE}(i_{\text{next}})$

exhibits a westward (negative) drift, which allows the admissible RAAN range to be bounded accordingly. Conversely, the inclination of a typical low Earth orbit at approximately 700 km altitude remains nearly constant over time, requiring only a narrow discretization range.

Let a, Ω, i, and ω denote the semi-major axis, RAAN, inclination, and argument of perigee, respectively, and let $\mathcal{S}_a$, $\mathcal{S}_\Omega$, $\mathcal{S}_i$, and $\mathcal{S}_\omega$ be the corresponding discrete sets of admissible values used to construct the orbit family O. The cardinality of the orbit family is then given by $|O| = |\mathcal{S}_a||\mathcal{S}_\Omega||\mathcal{S}_i||\mathcal{S}_\omega|$.

When a perfect lookup table is employed, the number of distinct orbits that can be indexed is bounded by $|O| \leq 2^b$, where b is the number of bits allocated in the dissemination frame. As a reference, allocating three bytes enables indexing up to $\approx 1.6 \times 10^7$ distinct orbits, which we will use as an upper-limit $|O|$ in our validation scenarios. The pseudo-algorithm applied from the satellite perspective is depicted in Alg. 1, while the frame reception and orbit determination from the device perspective can be observed in Alg. 2.

5 Validation and Results

The proposed dissemination strategy is evaluated using software simulations that combine high-fidelity propagation and event detection. Two entities are modeled: a satellite with *source-of-truth* orbital knowledge (generated using STK Astrogator HPOP v10) and a constrained End Device. The spacecraft is represented as a 6 kg CubeSat-class platform with 0.24 m^2 cross-sectional area, enabling realistic drag modeling [29, 32]. The End Device estimates visibility using Orekit's SGP4 with event detectors [23], reflecting the asymmetry between high-fidelity onboard knowledge and lightweight ground prediction.

Key assumptions for this evaluation are: successful frame reception during access; device activation at predicted rise without in-pass recomputation; impulsive maneuvers outside visibility; 5° elevation mask with passes shorter than one minute discarded; synchronized clocks (32-bit timestamps); identical initial orbital elements; and deferred recomputation after frame reception.

Three cases are compared: (i) **No update**; (ii) **Baseline**, transmitting full orbital elements (128 bits + ID); and (iii) **Proposed**, transmitting a 24-bit orbit identifier (56 bits + ID). Performance is evaluated over five days across two orbital scenarios, with rise/set time prediction error as the primary metric. The workflow is outlined in Fig. 3. The simulation workflow is summarized in Fig. 3.

Algorithm 3 Orbit Broadcast and Update Simulation

Require: True access intervals I_{HPOP}
Require: Device d with local orbit database $\mathcal{D}$
Require: Scenario timespan $[t_0, t_f]$, propagation step Δt
Ensure: Device-predicted access intervals I_{device}
Ensure: Satellite's initial orbit O_0

$d.O_{ref} \leftarrow O_0$ ▷ *Initialization*
$d.O_{last} \leftarrow O_0$
$I_{\text{device}} \leftarrow \textsc{ComputeAccess}(d, O_0, t_0, t_f, \Delta t)$ ▷ *Initial access prediction*
$\mathcal{I}_{\text{HPOP}} \leftarrow \textsc{LoadAccessIntervals}(\text{HPOP data})$ ▷ *Load HPOP computed accesses*
for each access interval $i \in I_{\text{HPOP}}$ **do**
    $t_i \leftarrow t_0 + i.\text{start}$
    $O_{approx} \leftarrow \textsc{SimplifyOrbit}(O_{true})$ ▷ *Prepare satellite broadcast*
    $e \leftarrow \textsc{EnumerateOrbit}(O_{approx})$
    $F \leftarrow \textsc{AssembleFrame}(e, S_{id}, T)$
    $\textsc{Broadcast}(F)$
    if T in i_{next} **then** $\textsc{Receive}(F)$ ▷ *Device update by enumeration*
        $O_{new} \leftarrow \mathcal{D}.\textsc{Lookup}(e)$
        if $O_{new} \neq \emptyset$ **then**
            $d.O_{last} \leftarrow O_{new}$
    $t_{\text{next}} \leftarrow t_0 + i.\text{end}$ ▷ *Recompute future access prediction*
    $I_{\text{device}} \leftarrow \textsc{ComputeAccess}(d, d.O_{last}, t_{\text{next}}, t_f, \Delta t)$

The first scenario corresponds to a near-polar orbit, while the second considers a low-inclination orbit. The resulting ground tracks and orbital geometries propagated in each case are illustrated in Fig. 1.

5.1 LacunaSat

The first validation scenario considers LacunaSat's mission launched in November 2025. This mission closely aligns with the target use case of the proposed orbit dissemination strategy, as it involves constrained devices communicating with a sparse satellite infrastructure used for remote DtS-IoT devices. We will use one of the mission's satellites as a reference, which was deployed as part of a shared mission aboard a Falcon 9 launch vehicle. Although Lacuna Space has not officially reported the final operational orbit of the spacecrafts, publicly available TLE data from Celestrak[1] indicate that the injected objects occupy a near-circular, retrograde orbit with an inclination of approximately 97.8° at an altitude of about 568 km, suggesting the intention to operate in a Sun-synchronous orbit. Two devices are deployed in remote locations: one in the south-west region of the United Kingdom, consistent with the company's reports on deployment locations for nodes in Great Britain [33], and the other on Elephant Island, near Antarctica. No orbital maneuvers will be considered for this satellite. The complete set of orbital elements adopted for this scenario, along with the simulation configuration parameters, is summarized in Fig. 2.

5.1.1 Orbital Elements Behavior and Enumeration

Both the mission's intended orbit and the resulting orbital element dynamics are used to generate the family of orbits that comprise the enumeration strategy. Over the five-day simulation period, the semi-major

[1] `https://celestrak.org`

Table 2: Reference Orbital Elements for LacunaSat Scenario

Start date (GMT)			End date (GMT)			Step [s]
21-01-2025 15:00:00.000			21-01-2026 15:00:00.000			15
Sat. ID	a [km]	e	i [deg]	Ω [deg]	ω [deg]	ν [deg]
1	6939.2967	0.001970	97.798	97.660	96.093	235.961
Dev. ID	Device latitude [deg]		Device longitude [deg]			
1	50.154764		-5.412035			

Table 3: Reference Orbital Elements for VLEO Scenario

Start date (GMT)			End date (GMT)			Step [s]
21-01-2025 15:00:00.000			21-01-2026 15:00:00.000			15
Sat. ID	a [km]	e	i [deg]	Ω [deg]	ω [deg]	ν [deg]
1	6678.137	0.000	28.500	120.000	0.000	120.000
Dev. ID	Device latitude [deg]		Device longitude [deg]			
1	-0.324222		-66.8293			

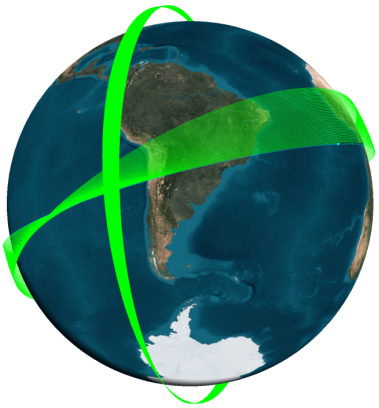

Figure 1: Illustration of the propagated orbital tracks for the two validation scenarios considered in this study, shown in an inertial reference frame.

axis exhibits almost no secular variation, and a similar behavior is observed for the eccentricity. The inclination, on the other hand, shows a more noticeable oscillation, although it remains well bounded within $\pm 0.02^\circ$ of the reference inclination. The RAAN is the predominantly varying orbital element in this case, drifting at a rate of approximately $\sim$1 deg/day, as expected for a Sun-synchronous orbit.

Orbit enumeration for the proposed strategy is achieved by populating a list containing all possible combinations of the reference orbit parameters: semi-major axis ± 25 km in 1 km steps, inclination $\pm 0.2^\circ$ in 0.025° steps, RAAN in the range $[-5^\circ, +20^\circ]$, and argument of latitude spanning the full 0°–360° range. This results in approximately 7×10^6 candidate orbits, which can be indexed with a 23-bit unsigned integer. Assuming 16-bit floating-point precision per enumerated element, and four such elements per orbit under our assumptions, the required storage is $4 \times 16 \times 7 \times 10^6$ bits. This corresponds to approximately 4.48×10^8 bits, i.e., about 56 MB of memory.

5.1.2 First Simulation: No Orbital Updates

The resulting rise and set time prediction errors for the first simulation are shown in Fig. 2. In this scenario, the device relies exclusively on its initial orbital knowledge and receives no subsequent orbital updates.

5.1.3 Second Simulation: Baseline Dissemination

In the second simulation, the device updates its orbital knowledge at each pass using a baseline dissemination frame that contains the complete set of orbital elements. The resulting rise and set time prediction errors are shown in Fig. 3.

The results reveal a clear accumulation of error across successive satellite passes in the absence of orbital updates, reaching approximately ten minutes after five days. This magnitude is comparable to the duration of a full access interval, effectively rendering access predictions unusable beyond this time horizon. When baseline dissemination is employed, prediction errors remain on the order of tens of seconds throughout the simulation period. Isolated error peaks are observed at intervals 7, 13, 19, and 25, which correspond to satellite passes occurring at very low elevation angles.

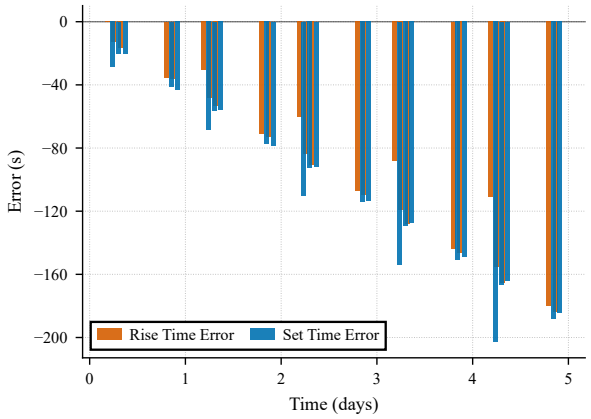

Figure 2: Rise and set time prediction errors when no orbital updates are performed after the initial deployment.

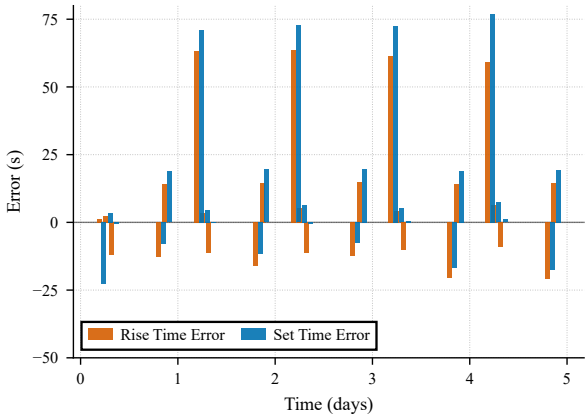

Figure 3: Rise and set time prediction errors when the full set of orbital elements is disseminated at each satellite pass.

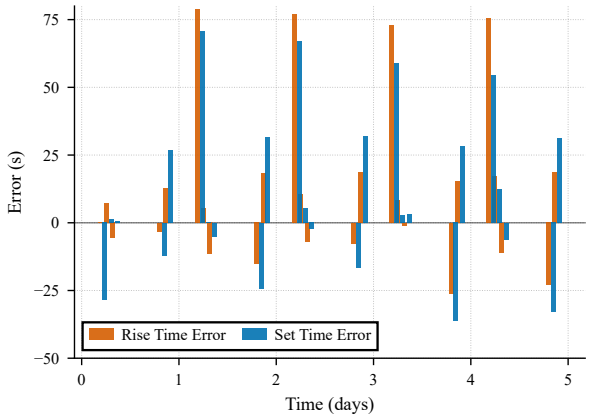

Figure 4: Rise and set time prediction errors when using the proposed orbit-family enumeration strategy.

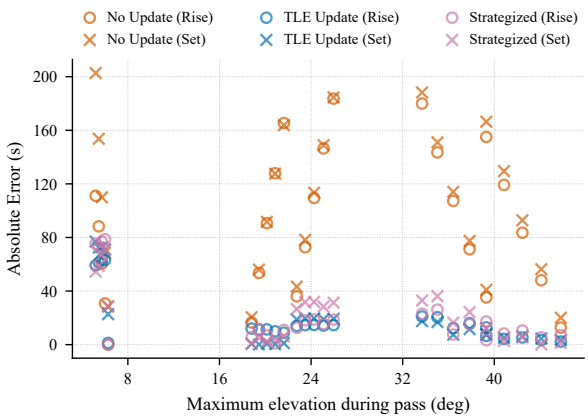

Figure 5: Rise and set time prediction errors (absolute) as a function of the maximum elevation achieved during each pass.

5.1.4 Third Simulation: Proposed Strategy

The results obtained when applying the proposed dissemination strategy are shown in Fig. 4.

As in the baseline case, error peaks are primarily observed during grazing passes near the horizon. Overall, the proposed strategy exhibits a modest increase in prediction error relative to full-element dissemination; however, the errors remain within the same order of magnitude and well below the threshold at which access prediction becomes impractical. To quantify the operational impact, aggregate metrics are computed in terms of (i) accumulated time active outside valid access windows (representing wasted energy) and (ii) accumulated time inactive during valid windows (representing channel underutilization). These results are summarized in Table 4.

Table 4: Aggregate timing error metrics and dissemination overhead for all evaluated scenarios. "Active Outside" denotes the accumulated time the device remained active outside valid access windows, while "Inactive During" denotes missed time within valid windows. "Allocated Memory" indicates storage required for orbit information on the End Device, and "Orbit Info Overhead" refers to aggregate transmitted orbit-update information size.

Scenario	Strategy	Active Outside Valid Windows [s]	Inactive During Valid Windows [s]	Allocated Memory [MB]	Orbit Info Overhead [bytes]
LacunaSat	No Update	2628.48	2248.71	Negligible	0
	TLE Update	428.29	553.57	Negligible	400
	Strategized	600.24	537.77	56	175
VLEO (1 Maneuver)	No Update	6736.94	6482.98	Negligible	0
	TLE Update	1081.30	865.25	Negligible	288
	Strategized	1332.09	1071.19	56	126
VLEO (4 Maneuvers)	No Update	5417.74	5360.34	Negligible	0
	TLE Update	1010.63	811.77	Negligible	384
	Strategized	1242.71	1024.36	56	168

5.2 VLEO Scenario

The second validation scenario considers a hypothetical very low Earth orbit (VLEO) satellite operating at an altitude of approximately 300 km. In this case, the ground device is assumed to be located at a remote, randomly selected position within the Amazon rainforest. The orbital and deployment parameters for this scenario are summarized in Fig. 3.

5.2.1 Orbital Elements Behavior

The overall analysis approach mirrors that of Sec. 5.1; however, due to the significantly lower orbital altitude, active orbit maintenance is required to counteract rapid orbital decay induced by atmospheric drag. Without such maneuvers, the satellite would reenter the atmosphere on a very short timescale.

Two maneuvering schemes are evaluated. In the first scheme, the satellite executes a single prograde impulse of 20 m/s at $t = 2.5$ days, followed by a smaller 2 m/s circularization maneuver half an orbit later. In the second scheme, the satellite performs four equally spaced prograde maneuvers at $t = 1$, 2, 3, and 4 days, each with a magnitude of 6.25 m/s. In both cases, all maneuvers are applied in the direction of the instantaneous velocity vector.

The evolution of the orbital elements during propagation exhibits the expected behavior for altitude-raising maneuvers in a drag-dominated VLEO regime. Figs. 6 and 7 illustrate the temporal evolution of the semi-major axis, eccentricity, inclination, and RAAN for the single-maneuver and multi-maneuver scenarios, respectively. The resulting rise and set time prediction errors, expressed as a function of the maximum elevation achieved during each access, are shown in Figs. 8 and 9 for the single- and multi-maneuver cases, respectively.

As in the LacunaSat case, prediction errors obtained using the proposed dissemination strategy remain within the same order of magnitude as those obtained when transmitting the full set of orbital elements. Notably, in the single-maneuver scenario, prediction accuracy degrades significantly after approximately the 17th access interval, at which point the predicted access windows no longer overlap with the actual line-of-sight intervals. This behavior highlights the increased sensitivity of VLEO missions to unmodeled orbital changes and underscores the importance of frequent orbital updates in drag-dominated regimes.

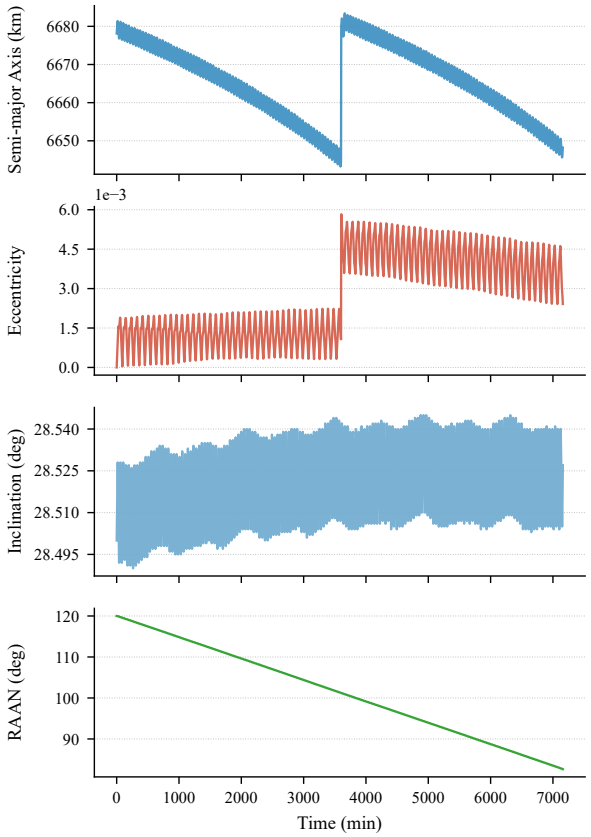

Figure 6: Orbital element evolution for the VLEO scenario with a single altitude-raising maneuver followed by a circularization burn.

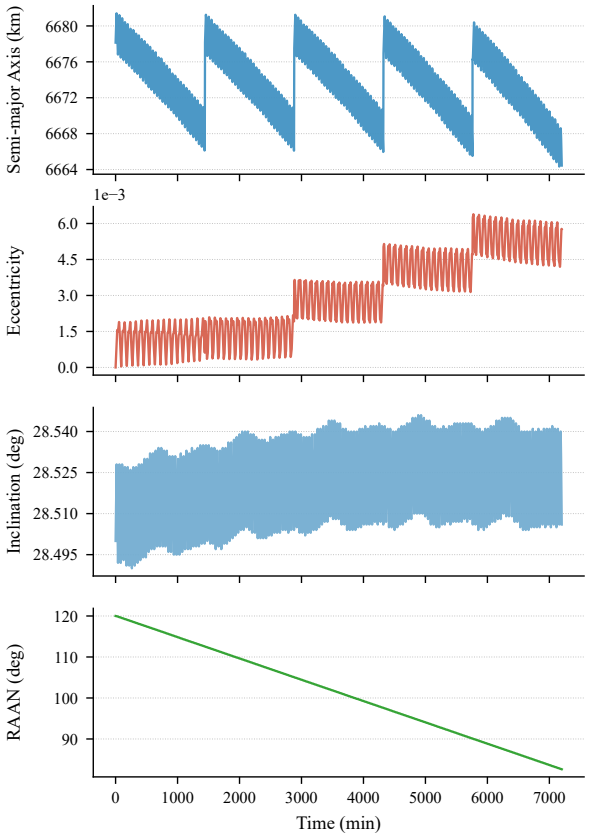

Figure 7: Orbital element evolution for the VLEO scenario employing four evenly spaced altitude-raising maneuvers.

As we did with the Lacuna Mission, aggregate metrics are computed to quantify the operational impact. These results are summarized in Table 4.

6 Conclusions

This work addressed the dissemination of orbit information to energy-constrained DtS-IoT devices under limited downlink capacity and reduced orbit predictability. An orbit-family enumeration strategy was introduced to compactly encode orbital updates, enabling devices to maintain access-interval prediction accuracy without transmitting full orbital element sets. Simulation results across a near-polar LEO scenario and a maneuvering VLEO scenario show that enumeration-based updates preserve rise and set time prediction errors within the same order of magnitude as baseline full-element dissemination, while reducing the payload overhead needed to disseminate the orbit by 56%. The results also underscore the sensitivity of VLEO operations to maneuver-driven state changes and the need for frequent updates in drag-dominated regimes.

- Orbit-family enumeration reduces the dissemination payload while preserving access-prediction accuracy comparable to full-element updates.

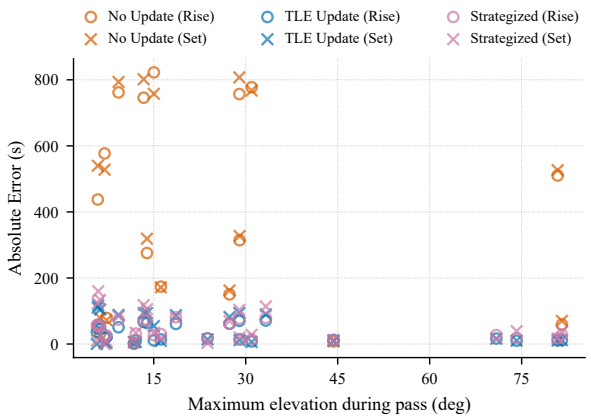

Figure 8: Rise and set time prediction errors as a function of maximum pass elevation for the VLEO scenario with a single maneuver.

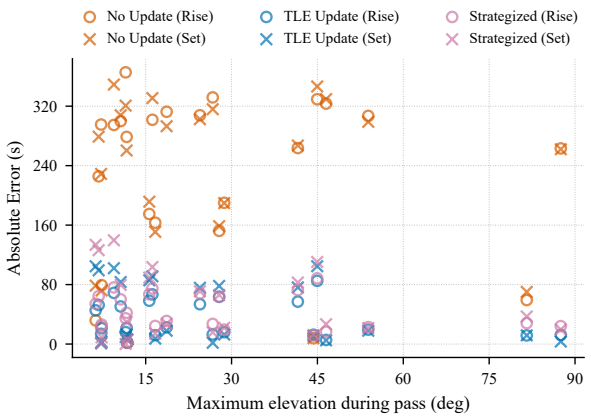

Figure 9: Rise and set time prediction errors as a function of maximum pass elevation for the VLEO scenario with four maneuvers.

- Prediction errors remain bounded for LEO scenarios without maneuvers but degrade quickly in maneuvering VLEO missions when orbital elements are not frequently disseminated.
- Enumeration-based updates provide a practical trade-off between update rate, information granularity, and device resource constraints.

Future work will focus on further reducing dissemination overhead through stronger modeling assumptions while quantifying the associated impact on prediction accuracy. Error behavior will be characterized across varying orbital family sizes to assess scalability. Additionally, the computational trade-off between on-demand reconstruction of orbital elements from a perturbation-encoding hash and the use of a precomputed hash-to-TLE lookup table will be investigated.

Acknowledgments

This project has received funding from the European Union's Horizon 2020 research and innovation programme under the Marie Skłodowska-Curie grant agreement No 101008233 (MISSION).

References

[1] Salvatore Alfano, David Negron Jr. & Jennifer L. Moore (1992): *Rapid Determination of Satellite Visibility Periods*. *The Journal of the Astronautical Sciences*. 40(2), pages 281–296. Available at `https://apps.dtic.mil/sti/pdfs/ADA267281.pdf`.

[2] Irfan Ali, Naofal Al-Dhahir & John E Hershey (1999): *Predicting the visibility of LEO satellites*. *IEEE Trans. Aerosp. Electron. Syst.* 35(4), pages 1183–1190, doi: `10.1109/7.805436`.

[3] Christopher S. Allen, Martina Giraudo, Claudio Moratto & Nobuyasu Yamaguchi (2018): *Chapter 4 – Spaceflight environment*. In *Space Safety and Human Performance*, chapter 4, pages 87–138. Butterworth-Heinemann, doi: `10.1016/B978-0-08-101869-9.00004-2`.

[4] Margo Anderson (2026): *CRASH Clock Measures Dangerous Overcrowding in Low Earth Orbit: One Solar Storm Could Trigger a Catastrophic Collision in Orbit*. *IEEE Spectrum*. Available at `https://spectrum.ieee.org/kessler-syndrome-crash-clock`.

[5] Argos System CLS: *ARGOS*. Available at https://www.argos-system.org/.

[6] Víctor Arroyo, Alicia Cordero & Juan R. Torregrosa (2011): *Approximation of artificial satellites' preliminary orbits: The efficiency challenge*. *Math. Comput. Model.* 54(7-8), pages 1802–1807, doi: 10.1016/J.MCM.2010.11.063.

[7] Guillem Boquet, Borja Martínez, Ferran Adelantado, Joan Pagès, Joan Adrià Ruiz-de-Azua & Xavier Vilajosana (2024): *Low-Power Satellite Access Time Estimation for Internet of Things Services Over Nonterrestrial Networks*. *IEEE Internet Things J.* 11(2), pages 3206–3216, doi: 10.1109/JIOT.2023.3298017.

[8] Richard L Branham (2005): *Laplacian orbit determination and differential corrections*. *Celestial Mech Dyn Astr*. 93(1), pages 53–68, doi: 10.1007/s10569-005-3242-6.

[9] Adrián Carlotto & José Juárez (2014): *Estudio sobre la Localización de Plataformas del sistema DCS del satélite SAC-D*. In *2014 IEEE Biennial Congress of Argentina (ARGENCON)*, IEEE, pages 722–726, doi: 10.1109/ARGENCON.2014.6868579.

[10] Giulio Colavolpe, Tommaso Foggi, Michelangelo Ricciulli, Yuri Zanettini & Juan Pedro Mediano Alameda (2019): *Reception of LoRa Signals From LEO Satellites*. *IEEE Trans. Aerosp. Electron. Syst.* 55(6), pages 3587–3602, doi: 10.1109/TAES.2019.2909336.

[11] Silvia Demetri, Marco Zúñiga, Gian Pietro Picco, Fernando A. Kuipers, Lorenzo Bruzzone & Thomas Telkamp (2019): *Automated estimation of link quality for LoRa: a remote sensing approach*. In *Proceedings of the 18th International Conference on Information Processing in Sensor Networks, IPSN 2019*, ACM, pages 145–156, doi: 10.1145/3302506.3310396.

[12] Alexander A. Doroshkin, Alexander M. Zadorozhny, Oleg N. Kus, Vitaliy Yu. Prokopyev & Yuri M. Prokopyev (2019): *Experimental Study of LoRa Modulation Immunity to Doppler Effect in CubeSat Radio Communications*. *IEEE Access*. 7, pages 75721–75731, doi: 10.1109/ACCESS.2019.2919274.

[13] Pedro Ramon Escobal (1963): *Rise and set time of a satellite about an oblate planet*. *AIAA Journal*. 1(10), pages 2306–2310, doi: 10.2514/3.2057.

[14] Vitor Fialho & Fernando Fortes (2020): *Battery Lifetime Estimation for LoRaWAN*. *International Journal of Innovative Technology and Exploring Engineering*. 9(11), pages 306–310, doi: 10.35940/ijitee.K7824.099112O.

[15] Juan A. Fraire, Sandra Céspedes & Nicola Accettura (2019): *Direct-To-Satellite IoT - A Survey of the State of the Art and Future Research Perspectives - Backhauling the IoT Through LEO Satellites*. In *Ad-Hoc, Mobile, and Wireless Networks - 18th International Conference on Ad-Hoc Networks and Wireless, ADHOC-NOW 2019, Proceedings*, *LNCS*, Springer, pages 241–258, doi: 10.1007/978-3-030-31831-4_17.

[16] Yi Gu, Chao Han & Xinwei Wang (2019): *A Kriging based framework for rapid satellite-to-site visibility determination*. In *2019 IEEE 10th International Conference on Mechanical and Aerospace Engineering (ICMAE)*, IEEE, pages 262–267, doi: 10.1109/ICMAE.2019.8880987.

[17] Chao Han, XiaoJie Gao & XiuCong Sun (2017): *Rapid satellite-to-site visibility determination based on self-adaptive interpolation technique*. *Sci. China Technol. Sci.* 60(2), pages 264–270, doi: 10.1007/s11431-016-0513-8.

[18] Chao Han, Pengbin Yang, Xiaohui Wang & Shenggang Liu (2018): *A fast computation method for the satellite-to-site visibility*. In *2018 IEEE Congress on Evolutionary Computation (CEC)*, IEEE, doi: 10.1109/CEC.2018.8477984..

[19] Chao Han, Yujin Zhang, Shengzhou Bai, Xiucong Sun & Xinwei Wang (2021): *Novel method to calculate satellite visibility for an arbitrary sensor field*. *Aerospace Science and Technology*. 112:106668, doi: 10.1016/j.ast.2021.106668.

[20] Lacuna Space (2025): *Lacuna Expands Direct-to-Device IoT Network with Successful "Call of the Wild" Satellite Launches*. Available at https://lacuna-space.com/lacuna-expands-direct-to-device-iot-network-with-successful-call-of-the-wild-satellite-launches/ (visited on 01/15/2026).

[21] Lacuna Space Ltd. (2023): *Lacuna LS200 Sensor and Relay: User Manual*, 2A8AP-LS300. Available at https://fcc.report/FCC-ID/2A8AP-LS300/6477923.pdf.

[22] Hugh G. Lewis & Donald J. Kessler (2025): *Critical Number of Spacecraft in Low Earth Orbit: A New Assessment of the Stability of the Orbital Debris Environment*. In *Proceedings of the 9th European Conference on Space Debris*, 1, ESA Space Debris Office. Available at https://conference.sdo.esoc.esa.int/proceedings/sdc9/paper/305.

[23] Luc Maisonobe, Véronique Pommier & Pascal Parraud (2010): *Orekit: an Open-source Library for Operational Flight Dynamics Applications*. In *4th International Conference on Astrodynamics Tools and Techniques, ICATT 2010*.

[24] Raydel Ortigueira, Samuel Montejo-Sánchez, Santiago Henn, Juan A. Fraire & Sandra Céspedes (2024): *Satellite Visibility Prediction for Constrained Devices in Direct-to-Satellite IoT Systems*. *IEEE Sensors Journal*. 24(16), pages 26630–26644, doi: 10.1109/JSEN.2024.3418728.

[25] Raditiana Patmasari, Inung Wijayanto, RS Deanto, YP Gautama & Hurianti Vidyaningtyas (2018): *Design and realization of automatic packet reporting system (APRS) for sending telemetry data in Nano satellite communication system*. *Journal of Measurements, Electronics, Communications, and Systems*. 4(1), doi: 10.25124/jmecs.v4i1.1692.

[26] Yubi Qian, Lu Ma & Xuwen Liang (2019): *The Acquisition Method of Symmetry Chirp Signal Used in LEO Satellite Internet of Things*. *IEEE Commun. Lett.* 23(9), pages 1572–1575, doi: 10.1109/LCOMM.2019.2926262.

[27] José Radzik & Gérard Maral (1995): *A Methodology for Rapidly Evaluating the Performance of Some Low Earth Orbit Satellite Systems*. *IEEE J. Sel. Areas Commun.* 13(2), pages 301–309, doi: 10.1109/49.345874.

[28] Siar Sarferaz (2022): *Internet of Things*. In *Compendium on Enterprise Resource Planning: Market, Functional and Conceptual View based on SAP S/4HANA*, chapter 25, pages 389–400. Springer, doi: 10.1007/978-3-030-93856-7_25.

[29] C Scharlemann, M Tajmar, I Vasiljevich, N Buldrini, D Krejci & B Seifert (2011): *Propulsion for nanosatellites*. In *32nd International Electric Propulsion Conference (IEPC 2011)*, IEPC-2011-171.

[30] Starlink: *Standard Kit Specification Sheet*. Available at https://starlink.com/specifications (visited on 01/15/2026).

[31] Xiucong Sun, Hongzheng Cui, Chao Han & Geshi Tang (2012): *APCHI technique for rapidly and accurately predicting multi-restriction satellite visibility*. In *Proceedings of the 22nd AAS/AIAA Space Flight Mechanics Meeting. Charleston, South Carolina*, pages 212–216.

[32] The Things Network Global Team (2020): *LoRa World Record Broken: 832km using 25mW*. Available at https://www.thethingsnetwork.org/article/lorawan-world-record-broken-twice-in-single-experiment-1 (visited on 05/29/2020).

[33] UK Space Agency Blog (2025): *Whispers from the Wild: Building Satellites that Listen to the Planet*. Available at https://space.blog.gov.uk/2025/06/25/whispering-to-the-wild-building-satellites-that-listen-to-the-planet/ (visited on 01/15/2026).

[34] David Vallado, Paul Crawford, Ricahrd Hujsak & T.S. Kelso (2006): *Revisiting Spacetrack Report #3*. In *AIAA/AAS Astrodynamics Specialist Conference and Exhibit*. AIAA, doi: 10.2514/6.2006-6753.

[35] David A. Vallado & Wayne D. McClain (2013): *Fundamentals of astrodynamics and applications*, 4th ed. Microcosm Press.

[36] J. R. Wertz (2001): *Mission Geometry; Orbit and Constellation Design and Management*, 1st edition, pages 58, 459. *Space Technology Library*, Springer Dordrecht. ISBN: 978-0-7923-7148-9.